Inhomogeneous vortex-state-driven enhancement of superconductivity in nanoengineered ferromagnet-superconductor heterostructures

R. K. Rakshit,[1] R. C. Budhani,[1,*] T. Bhuvana,[2] V. N. Kulkarni,[3] and G. U. Kulkarni[2]
[1]*Condensed Matter-Low Dimensional Systems Laboratory, Department of Physics, Indian Institute of Technology Kanpur, Kanpur 208016, India*
[2]*Jawaharlal Nehru Centre for Advanced Scientific Research, Jakkur Post Office, Bangalore 560064, India*
[3]*Central Nuclear Laboratory, Department of Physics, Indian Institute of Technology Kanpur, Kanpur 208016, India*
(Received 15 November 2007; published 28 February 2008)

Thin film heterostructures provide a powerful means to study the antagonism between superconductivity (SC) and ferromagnetism (FM). One interesting issue in FM-SC hybrids, which defies the notion of antagonistic orders, is the observation of magnetic field-induced superconductivity (FIS). Here, we show that in systems where the FM domains and/or islands produce spatial inhomogeneities of the SC order parameter, the FIS can derive significant contribution from different mobilities of the magnetic flux identified by two distinct critical states in the inhomogeneous superconductor. Our experiments on nanoengineered bilayers of ferromagnetic CoPt and superconducting NbN, where CoPt/NbN islands are separated by a granular NbN, lend support to this alternative explanation of FIS in certain class of FM-SC hybrids.

DOI: 10.1103/PhysRevB.77.052509 PACS number(s): 74.78.Fk, 74.25.Qt, 74.62.−c, 75.75.+a

The pinning of magnetic flux lines in a superconducting (SC) film by ferromagnetic (FM) dots and multidomain magnetic films has been a topic of considerable interest.[1–8] An important consequence of the inhomogeneous magnetic field produced by such structures is the formation of a local field-free state when the FM-SC hybrid is placed in an external magnetic field. This effect has been variously called as field-enhanced superconductivity,[1,2] magnetization controlled superconductivity,[3] and domain wall superconductivity.[4,5]

Earlier studies of FM-SC hybrids have been carried out mostly on films of elemental superconductor such as Nb and Pb deposited on in plane as well as high coercivity perpendicular anisotropy media.[1–8] Although striking field-induced changes in the critical temperature (T_c) of the superconductor have been seen, the field-free regions produced by the dipolar field of FM dots are not homogeneous in these systems. Also, it is not clear whether superconductivity actually survives in areas above (or below) the dots because of the small upper critical field (H_{c2}) of the elemental superconductors and strong magnetization of the dots. The global superconducting order parameter in these FM-SC hybrids is clearly inhomogeneous irrespective of the orientation of magnetization in the dots. It is therefore important to address the possible role of granularity in causing the field induced superconductivity (FIS) in such systems. The relevance of this issue becomes apparent from the richness of the field-temperature (H-T) phase diagram of well-known granular systems such as composite films,[9] high T_c ceramics,[10] and Josephson-junction arrays.[11]

In this Brief Report, we address field-induced superconductivity in nanoengineered grids of CoPt/NbN where the CoPt-free regions have been made granular, with a reduced T_c. The advantage of using NbN is in its large H_{c2} (>250 kOe) which prohibits a significant perturbation of superconductivity by the CoPt. The resistance (R) of the nanoengineered structures has been measured with current density $J \geqslant J_c$ as a function of external field $\vec{H}$ applied in two different orientations: (i) $(\vec{H} \perp \vec{J}) \perp \hat{n}$ and (ii) $(\vec{H} \| \vec{J}) \perp \hat{n}$, where $\hat{n}$ is a unit vector normal to the plane of the film. The R vs H loops are hysteretic with their reverse branch showing entry into the superconducting state at fields much higher than the field at which R appears in the forward branch. This FIS state is shown to be a consequence of the granularity of magnetic and superconducting order parameters in the hybrid.

Thin film bilayers of CoPt and NbN, each has 50 nm thick, were deposited on (001) MgO at 600 °C using pulsed laser ablation of CoPt and Nb targets, respectively. Further details of the deposition of NbN and CoPt films are given elsewhere.[12–14] The bilayer film was first patterned with standard lithography and then Ar^+ ion milled into a $100 \times 500\ \mu m^2$ bridge, as shown in Fig. 1. The top CoPt layer was then structured in simple square patterns using a Ga^{3+} focused ion beam (FIB) milling facility. Figure 1(b) shows a typical scanning electron micrograph of the patterned bilayer. The size of each CoPt element in the pattern is $0.5 \times 0.5\ \mu m^2$ with 50 nm spacing in between. The active area of the sample on which transport measurements were carried out contains 10×210 square elements.

The magnetic domain structure of the CoPt squares was probed with magnetic force microscopy (MFM) and atomic force microscopy (AFM) performed simultaneously on a thermally demagnetized sample in the tapping mode at various lift heights. A commercial magnetometer was used for measurement of magnetization. The critical current density (J_c), resistance R (T), and magnetoresistance R (H) were measured between 5 and 20 K.

Since the central result of this Brief Report is based on inhomogeneities of the SC and FM order parameters, we first establish these inhomogeneities in the patterned sample. Figure 2 presents R (T) of the patterned as well as unpatterned bilayer. While the latter film shows a sharp transition ($\Delta T \approx 0.5$ K) with T_c onset at ≈15.3 K, the R (T) of the patterned film exhibits a two-step structure—where the first drop in resistance occurs at ≈15.1 K in which R decreases by ≈60% of its normal state value. The second transition

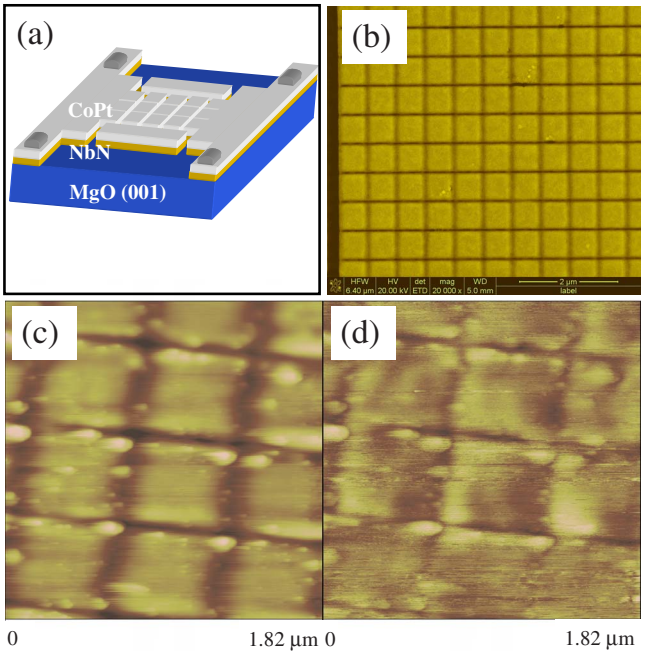

FIG. 1. (Color online) A schematic of the sample design is shown in panel (a). Panel (b) shows a scanning electron micrograph of the patterned bilayer and panels (c) and (d) AFM and MFM images, respectively. AFM and MFM measurements were performed simultaneously on thermally demagnetized samples at lift height of 40 nm. AFM image of the sample is quite similar to its scanning electron microscopy image. The bright and dark features in MFM represent domains of reversed magnetization.

starts at ≈13 K, culminating in $R=0$ at ≈11.8 K. The change from single-step to two-step transition on nanostructuring is presumably a result of Ga^{3+} ion damage. This feature, however, provides the unique advantage of addressing

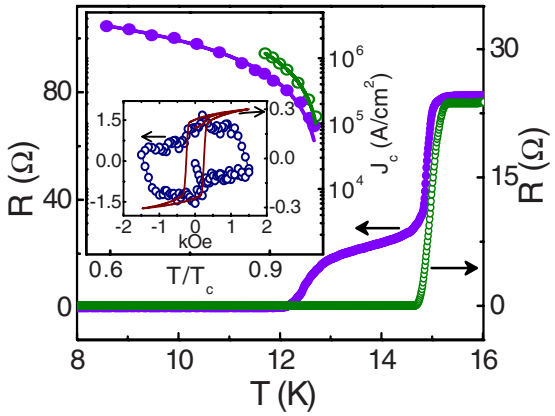

FIG. 2. (Color online) R (T) of the patterned (filled circles) and unpatterned (open circles) bilayers. A clear two-step superconducting transition is seen in the patterned film. The inset shows J_c of the unpatterned (open circles) and patterned (solid circles) samples. M vs H loops for an unpatterned bilayer sample at 5 K (open symbols) and 20 K (solid line), with field applied parallel to the film surface, are also shown in the inset. Here, the magnetization is measured in the unit of 10^{-3} emu.

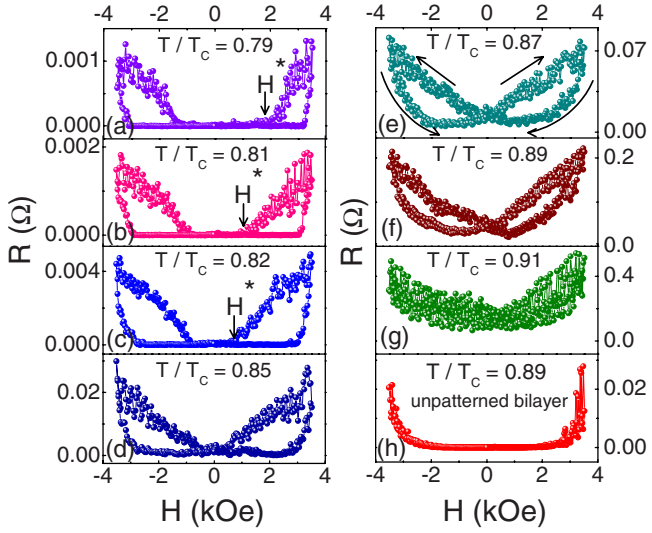

FIG. 3. (Color online) R (H) of the nanoengineered CoPt-NbN/MgO bilayer is shown in panels (a)–(g) at several T/T_c. Small arrows in panel (e) mark the direction of field sweep. The critical field H^* at which dissipation appears on ramping the field from zero has also been marked in the figures with vertical arrows. Panel (h) shows R (H) of the unpatterned sample at T/T_c=0.89.

FIS in a granular medium. The inset of Fig. 2 compares the J_c (T) of the nanostructured and a plane bilayer film. The J_c of the unpatterned film quickly reaches the limit of our measurement which is set by the width of the bridge and maximum current used (≈100 mA). However, a pronounced reduction in the J_c is seen on nanopatterning. Since the capacity of such structures to carry dissipation less current is determined by their low T_c links, a suppressed growth of J_c on lowering the temperature indicates that the channels of NbN connecting CoPt/NbN islands are granular.

Figure 2 also shows magnetization (M) of an unpatterned bilayer at 5 and 20 K as a function of magnetic field applied along the surface of the film. The square hysteresis loop of low coercivity (≈250 Oe) at 20 K seen here suggests a soft ferromagnetic state in CoPt with in-plane $\vec{M}$, a characteristic feature of the disordered fcc phase of CoPt.[13] The M-H curve traced at 5 K is dominated by the diamagnetic response of the NbN layer. While it was not possible to measure the magnetic state of the patterned film with superconducting quantum interference device magnetometry, we have used room temperature MFM to visualize domain structure of the CoPt islands. Figures 1(c) and 1(d) show the AFM and MFM micrographs, respectively, taken from the same spot on the film.[15] The bright and dark features in MFM represent domains of reversed $\vec{M}$. Since each patterned CoPt island has two such domains, it is clear that they are in a thermally demagnetized state.

In Fig. 3, we show a set of R (H) data for the nanostructured film at several T/T_c, where T_c is the temperature (≈11.8 K) at which zero-resistance state is reached. The magnetic field applied in the plane of the film and orthogonal to current in these measurements was scanned in the unit of kOe following the cycle $0\rightarrow 3.5\rightarrow 0\rightarrow -3.5\rightarrow 0$. A constant

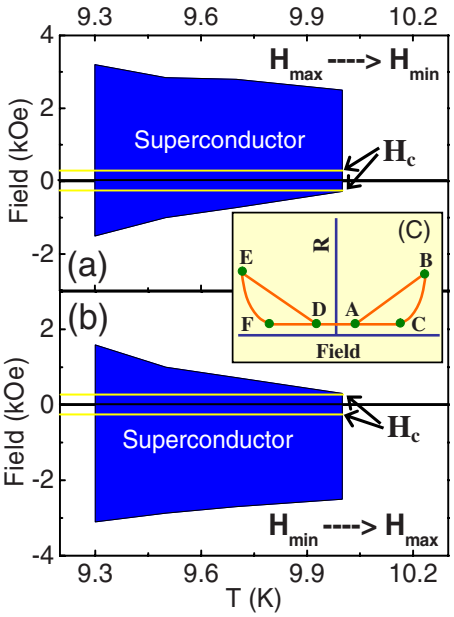

FIG. 4. (Color online) The dark areas in panels (a) and (b) show the H-T phase space where the FIS exists, as shown by results of Fig. 3. Panel (c) sketches the R-H curve in which critical points have been marked by letters A, B, C, D, E, and F. The contours of points C and D as a function of temperature are shown in (a) while scanning the field from $+H_{max}$ to $-H_{max}$. Contours of points F and A are shown in panel (b) for the field scan from $-H_{max}$ to $+H_{max}$. The coercive field $H_c = \pm 250$ Oe is drawn by a pair of horizontal lines in both the phase diagrams.

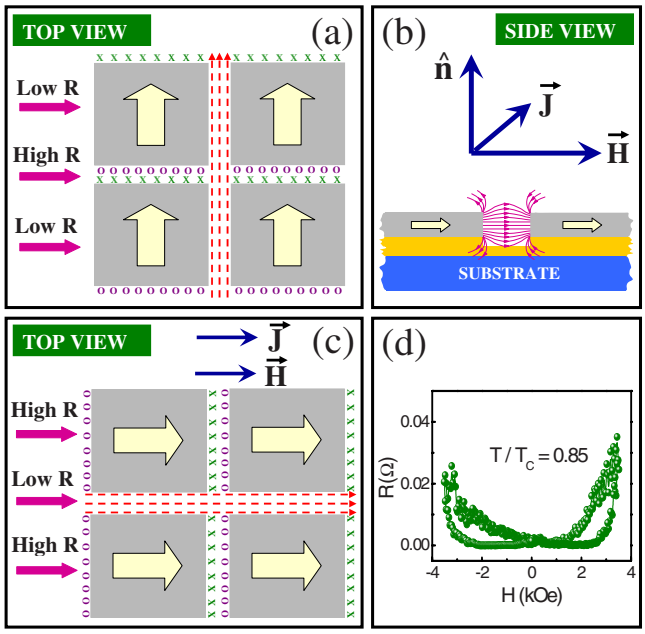

FIG. 5. (Color online) Panel (a): top view of flux distribution for $(\vec{H} \perp \vec{J}) \perp \hat{n}$. In-plane field lines are shown as dotted lines, whereas the dipolar field penetrating the NbN channel is shown by circles and crosses. Large arrows in the middle of squares mark the direction of $\vec{M}$ of CoPt islands. A side view of the dipolar field produced by the CoPt is sketched in panel (b). Panel (c) shows the flux distribution when $\vec{H}$ and $\vec{J}$ are collinear. Panel (d) shows R vs H plot in $\vec{H} \| \vec{J}$ configuration at $T/T_c = 0.85$.

current density of 1×10^6 A/cm^2, which corresponds to the J_c at 9.8 K (T/T_c=0.83), was used for resistance measurements. At small T/T_c (=0.79), the R first remains zero with the increasing field. This is expected as the zero-field current density J is smaller than the J_c at this T/T_c. However, as the field increases, J_c drops and at $H=H^*$ (marked in the figure), the J becomes larger than J_c and the sample goes in a dissipative state. Here, the dependence of R is linear on H, as expected in the flux flow regime of the mixed state. On reversing the field, however, the resistance drops to zero much faster. The dissipationless state appears at a higher field H ($>H^*$) in the reverse branch of the loop. A similar hysteretic behavior is seen at the higher values of T/T_c. In Fig. 3(h), we show the result of a similar measurement performed on an unpatterned bilayer. In this case, the R vs H curve is completely reversible. It is clear from these measurements that the hysteretic behavior of R vs H is a consequence of the nanopatterning. This is the central result of our Brief Report.

In Figs. 4(a) and 4(b), we summarize these observations of a field-assisted reentrant superconducting state in terms of H-T phase diagram. Figure 4(c) shows a sketch of the R-H curve whose critical points have been marked by letters A, B, C, D, E, and F. Point A corresponds to H^* where superconductivity disappears on ramping up the field, point B denotes the maximum applied field, and point C is where superconductivity reappears on reducing the field from its maximum value. Similarly, points D and F mark destruction and reappearance of SC on the reverse branch of the loop, while E corresponds to the maximum negative field. The contours of points C and D as a function of temperature are shown in Fig. 4(a), and the shaded area enclosed by them is the range of field where global superconductivity exists while scanning it from $+H_{max}$ to $-H_{max}$. Figure 4(b) is the phase space of superconductivity for $-H_{max}$ to $+H_{max}$ excursion.

Before attempting to set forward a model which would allow us to understand the results of Figs. 3 and 4, it is important to point out that for our film of thickness d ($\approx$50 nm), much smaller than the penetration depth λ ($\approx$200–250 nm) placed in a parallel field, a large contribution to dissipation may come from orbital and Pauli pair-breaking processes, in addition to the dissipation due to flux flow. However, the pair-breaking processes are not hysteretic. The misalignment of the magnetic field away from a true parallel configuration is also an important issue because the parasitic out-of-plane component of the field can lead to nucleation of perpendicular vortices. To rule out this possibility, we had aligned the field parallel to the plane of the film with a precision of $\pm 0.1°$ using a specially built experimental setup.[16]

A correct model for understanding the phase diagram of Fig. 4 must take into account two important features of the nanostructured sample; first, it has a periodic granularity. The CoPt-NbN squares become superconducting at $\approx$15.1 K, but a long-range phase coherence develops only when the CoPt-free grids go superconducting at $\approx$11.8 K. The patterned

film therefore is characterized by two distinct critical current densities: a large J_{cg} inside the NbN-CoPt squares and a much weaker J_{cj} in the channels separating these squares. Second, the CoPt islands have in-plane $\vec{M}$ with coercive field of ≈250 Oe (see Fig. 2), which has been marked by a pair of horizontal lines in the phase diagram of Fig. 4. It is clear that in most of the phase space, the CoPt islands are saturated with their $\vec{M} \| \vec{H}$. A qualitative understanding of the flux distribution can be made from Figs. 5(a) and 5(c) drawn for $(\vec{H} \perp \vec{J}) \perp \hat{n}$ and $(\vec{H} \| \vec{J}) \perp \hat{n}$ configurations. We show that even when CoPt squares are flux coupled at $H > H_c$, some fringing field from the edges of the squares produces flux lines of opposite polarity in the NbN channels. These are marked by open circles and crosses in the top view of the square array. The flux due to external magnetic field has a different distribution in the channels and the CoPt covered NbN squares because of their different J_c. It can be understood in the framework of the two-level critical state model of Ji *et al.*[17] Using this model we can define two types of fluxons: (i) those pinned by pinning centers in the square (ϕ_p) and (ii) the fluxons that are confined to the channels and are free to move due to weak pinning (ϕ_f). As the external field is increased, fluxons enter the channels first, supersaturating them and leading to the increase of dissipation along A-B branch of the curve in Fig. 4(c). The flux eventually enters the squares where it is pinned. On decreasing the field, the free flux (ϕ_f) leaks out from the channels to such an extent that the zero-resistance state is reestablished along the low resistance paths marked in Fig. 5 at a higher value of the external field. This is possible because there is a large pinned flux (ϕ_p) in the NbN squares.

We expect that in the $\vec{H} \perp \vec{J}$ configuration [Fig. 5(a)], the current flow along the channels (paths which do not cross CoPt-NbN squares) remains dissipative due to the dipolar field of CoPt. This is where the magnetization of CoPt plays an explicit role. A similar scenario also explains reentrant superconductivity seen for the $\vec{H} \| \vec{J}$ configuration sketched at the left bottom panel (c) of Fig. 5. A typical set of R vs H data taken at $T/T_c = 0.85$ in $\vec{H} \| \vec{J}$ configuration is shown in panel (d) of Fig. 5. The granular NbN channels although form a continuous path for the flow of current for $\vec{H} \| \vec{J}$, the cores of vortices, which are already large due to a small order parameter in the channels, start overlapping, and even at low fields, the channels become resistive. The onset of resistance here has nothing to do with vortex motion under the Lorentz force. This type of force-free dissipation has been seen in granular films of NbN.[18]

The observations made in the present study have important repercussions on the phenomenon of field-assisted superconductivity seen in FM-SC bilayers,[19] trilayers,[20] and dot structures.[2] While in the case of FM-SC-FM trilayer structures placed in an in-plane field, no inhomogeneity of the order parameter is introduced as long as each FM layer behaves like a single domain film; the same is unavoidable in bilayers at field $H < H_c$ and in dot arrays even beyond saturation. We believe that in such systems, the repercussions of the two-level critical state model warrant consideration.

This research has been supported by a grant from the Nanoscience & Nanotechnology Initiative of the Department of Science & Technology, Government of India, and internal funding of IIT Kanpur. We thank G. K. Mehta for his support in setting up the FIB facility and S. K. Bose, R. Sharma, and S. Srivastava for technical assistance.

*rcb@iitk.ac.in

[1] I. F. Lyuksyutov and V. L. Pokrovsky, Adv. Phys. **54**, 67 (2005).
[2] M. Lange, M. J. Van Bael, Y. Bruynseraede, and V. V. Moshchalkov, Phys. Rev. Lett. **90**, 197006 (2003).
[3] I. F. Lyuksyutov and V. Pokrovsky, Phys. Rev. Lett. **81**, 2344 (1998).
[4] A. Yu. Aladyshkin, A. I. Buzdin, A. A. Fraerman, A. S. Mel'nikov, D. A. Ryzhov, and A. V. Sokolov, Phys. Rev. B **68**, 184508 (2003).
[5] W. Gillijns, A. Y. Aladyshkin, M. Lange, M. J. Van Bael, and V. V. Moshchalkov, Phys. Rev. Lett. **95**, 227003 (2005).
[6] D. Stamopoulos, M. Pissas, V. Karanasos, D. Niarchos, and I. Panagiotopoulos, Phys. Rev. B **70**, 054512 (2004).
[7] D. J. Morgan, and J. B. Ketterson, Phys. Rev. Lett. **80**, 3614 (1998).
[8] M. J. Van Bael, J. Bekaert, K. Temst, L. van Look, V. V. Moshchalkov, Y. Bruynseraede, G. D. Howells, A. N. Grigorenko, S. J. Bending, and G. Borghs, Phys. Rev. Lett. **86**, 155 (2001).
[9] I. S. Beloborodov, A. V. Lopatin, V. M. Vinokur, and K. B. Efetov, Rev. Mod. Phys. **79**, 469 (2007).
[10] M. Tinkham and C. J. Lobb, in *Solid State Physics*, edited by H. Ehrenreich and D. Turnbull (Academic, San Diego, 1989), Vol. 42, p. 91.
[11] P. Martinoli and C. T. Leemann, Low Temp. Phys. **118**, 699 (2000).
[12] R. K. Rakshit, S. K. Bose, R. Sharma, and R. C. Budhani, Appl. Phys. Lett. **89**, 202511 (2006).
[13] R. K. Rakshit, S. K. Bose, R. Sharma, R. C. Budhani, T. Vijaykumar, S. J. Neena, and G. U. Kulkarni, J. Appl. Phys. **103**, 023915 (2008).
[14] K. Senapati, N. K. Pandey, R. Nagar, and R. C. Budhani, Phys. Rev. B **74**, 104514 (2006).
[15] Simultaneous sampling of magnetic and topographic images at different lift heights (even up to 120 nm) ruled out any topographical artifact presents in MFM image.
[16] S. Patnaik, K. Singh, and R. C. Budhani, Rev. Sci. Instrum. **70**, 1494 (1999).
[17] L. Ji, M. S. Rzchowski, N. Anand, and M. Tinkham, Phys. Rev. B **47**, 470 (1993).
[18] D. H. Kim, K. E. Gray, R. T. Kampwirth, K. C. Woo, D. M. McKay, and J. Stein, Phys. Rev. B **41**, 11642 (1990).
[19] A. Y. Rusanov, M. Hesselberth, J. Aarts, and A. I. Buzdin, Phys. Rev. Lett. **93**, 057002 (2004).
[20] J. Y. Gu, C.-Y. You, J. S. Jiang, J. Pearson, Y. B. Bazaliy, and S. D. Bader, Phys. Rev. Lett. **89**, 267001 (2002).